Higher Order Interpolatory Vector Bases on Prism Elements

Roberto D. Graglia, *Fellow, IEEE*, Donald R. Wilton, *Fellow, IEEE*, Andrew F. Peterson, *Senior Member, IEEE*, and Ioan-Ludovic Gheorma

***Abstract*— Triangular prism elements are useful in numerical solutions of electromagnetic field problems since they permit a three-dimensional (3-D) geometry to be generated by the extrusion of a triangular mesh. To date, however, few applications have employed vector basis functions on prism elements and the extension to distorted prisms reported in the literature apparently does not ensure cell-to-cell continuity. In this paper, we define interpolatory higher order curl- and divergence-conforming vector basis functions of the Nedelec type on prism elements, with extension to curved prisms, and discuss their completeness properties. Vector bases of arbitrary polynomial order are given and various results to confirm the faster convergence of higher order functions are presented.**

***Index Terms*— Electromagnetic fields, finite-element methods, numerical analysis.**

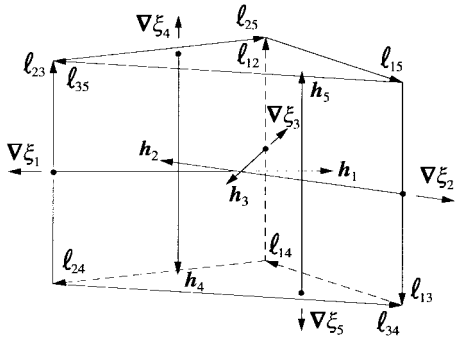

Fig. 1. Edge, height, and gradient vectors for prism elements.

I. Introduction

RECENTLY [1], we presented a unified and consistent procedure for defining interpolatory higher order vector basis functions of the Nedelec variety [2] for the most common element shapes. The procedure has been presented for triangular and quadrilateral elements in two dimensions and for tetrahedral and brick elements in three dimensions. In this paper, we apply the same procedure to define higher order interpolatory vector bases on prism elements. For an exhaustive treatise on vector bases for all these elements the reader is referred to [3]. Here, for prism elements, we consider both curl- and divergence-conforming bases, which have continuous tangential or normal components, respectively, across adjacent elements. Curl conforming basis functions are appropriate for discretizing the vector Helmholtz operator, while divergence conforming functions are appropriate for integral operators such as the electric field integral equation. These bases avoid the spurious modes usually encountered when scalar representations are used with one of the foregoing equations and simplify the enforcement of boundary conditions on current or fields in a numerical approach.

Manuscript received July 24, 1997; revised November 26, 1997. This work was supported in part by the Italian National Research Council (CNR) under Grant 07/97.00938, the Italian Ministry of University and Scientific Research, the Sandia National Laboratories, Albuquerque, NM, under Contract AN9938, and by the National Science Foundation under Grant ECS-9257927.

R. D. Graglia and I.-L. Gheorma are with the Dipartimento di Elettronica, Politecnico di Torino, Torino, 10129 Italy.

D. R. Wilton is with the Department of Electrical and Computer Engineering, University of Houston, Houston, TX 77204 USA.

A. F. Peterson is with the School of Electrical and Computer Engineering, Georgia Institute of Technology, Atlanta, GA 30332 USA.

Publisher Item Identifier S 0018-926X(98)02269-8.

In numerical applications, prism elements are particularly convenient for discretizing finite layered structures of different materials such as conformal patch antennas or arrays [4]. In such cases, the structure can be discretized using a two-dimensional (2-D) mesher to define triangular cells on one surface of a layer boundary; the three-dimensional (3-D) mesh is then obtained by extruding the triangles into prism cells. In contrast to [4], the curl-conforming prism elements presented here provide cell-to-cell tangential continuity even in the curvilinear case.

II. Element Geometry Representation

In this section, we define normalized parametric coordinates and related geometrical quantities by assuming rectilinear prism elements; extension to curvilinear elements is easily obtained by use of the results of [1, Appendix]. The geometrical parameters for prism elements are shown in Fig. 1. The faces are numbered to correspond to the indexing of the associated parametric coordinates; that is, the ith face of the prism is the zero-coordinate surface for the normalized coordinate ξ_i, which varies linearly across the element, attaining a value of unity at the edge or face opposite the zero-coordinate surface. For the prism element we choose as *independent* coordinates ξ_1, ξ_2, and ξ_4, so that $\nabla\xi_4 \cdot (\nabla\xi_1 \times \nabla\xi_2)$ is strictly positive, while ξ_3 and ξ_5 are *dependent* coordinates. In this case, the dependency relations are

$$\begin{aligned} \xi_1 + \xi_2 + \xi_3 &= 1 \\ \xi_4 + \xi_5 &= 1. \end{aligned} \tag{1}$$

0018–926X/98$10.00 © 1998 IEEE

TABLE I
ZEROTH-ORDER BASES ON PRISM ELEMENTS

curl-conforming bases		divergence-conforming bases
$\boldsymbol{\Omega}_{14}(\boldsymbol{r})=\xi_5(\xi_2\nabla\xi_3-\xi_3\nabla\xi_2)$	$\nabla\times\boldsymbol{\Omega}_{14}(\boldsymbol{r})=\frac{1}{\mathcal{J}}(\xi_3\boldsymbol{\ell}_{25}-\xi_2\boldsymbol{\ell}_{35}+2\xi_5\boldsymbol{\ell}_{23})$	
$\boldsymbol{\Omega}_{15}(\boldsymbol{r})=\xi_4(\xi_3\nabla\xi_2-\xi_2\nabla\xi_3)$	$\nabla\times\boldsymbol{\Omega}_{15}(\boldsymbol{r})=\frac{1}{\mathcal{J}}(\xi_2\boldsymbol{\ell}_{34}-\xi_3\boldsymbol{\ell}_{24}-2\xi_4\boldsymbol{\ell}_{23})$	
$\boldsymbol{\Omega}_{24}(\boldsymbol{r})=\xi_5(\xi_3\nabla\xi_1-\xi_1\nabla\xi_3)$	$\nabla\times\boldsymbol{\Omega}_{24}(\boldsymbol{r})=\frac{1}{\mathcal{J}}(\xi_1\boldsymbol{\ell}_{35}-\xi_3\boldsymbol{\ell}_{15}-2\xi_5\boldsymbol{\ell}_{13})$	$\boldsymbol{\Lambda}_1(\boldsymbol{r})=\frac{1}{\mathcal{J}}(\xi_2\boldsymbol{\ell}_{34}-\xi_3\boldsymbol{\ell}_{24})$
$\boldsymbol{\Omega}_{25}(\boldsymbol{r})=\xi_4(\xi_1\nabla\xi_3-\xi_3\nabla\xi_1)$	$\nabla\times\boldsymbol{\Omega}_{25}(\boldsymbol{r})=\frac{1}{\mathcal{J}}(\xi_3\boldsymbol{\ell}_{14}-\xi_1\boldsymbol{\ell}_{34}+2\xi_4\boldsymbol{\ell}_{13})$	$\boldsymbol{\Lambda}_2(\boldsymbol{r})=\frac{1}{\mathcal{J}}(\xi_3\boldsymbol{\ell}_{14}-\xi_1\boldsymbol{\ell}_{34})$
$\boldsymbol{\Omega}_{34}(\boldsymbol{r})=\xi_5(\xi_1\nabla\xi_2-\xi_2\nabla\xi_1)$	$\nabla\times\boldsymbol{\Omega}_{34}(\boldsymbol{r})=\frac{1}{\mathcal{J}}(\xi_2\boldsymbol{\ell}_{15}-\xi_1\boldsymbol{\ell}_{25}+2\xi_5\boldsymbol{\ell}_{12})$	$\boldsymbol{\Lambda}_3(\boldsymbol{r})=\frac{1}{\mathcal{J}}(\xi_1\boldsymbol{\ell}_{24}-\xi_2\boldsymbol{\ell}_{14})$
$\boldsymbol{\Omega}_{35}(\boldsymbol{r})=\xi_4(\xi_2\nabla\xi_1-\xi_1\nabla\xi_2)$	$\nabla\times\boldsymbol{\Omega}_{35}(\boldsymbol{r})=\frac{1}{\mathcal{J}}(\xi_1\boldsymbol{\ell}_{24}-\xi_2\boldsymbol{\ell}_{14}-2\xi_4\boldsymbol{\ell}_{12})$	$\boldsymbol{\Lambda}_4(\boldsymbol{r})=\frac{\xi_5\boldsymbol{\ell}_{13}}{\mathcal{J}}$
$\boldsymbol{\Omega}_{13}(\boldsymbol{r})=\xi_2\nabla\xi_5$	$\nabla\times\boldsymbol{\Omega}_{13}(\boldsymbol{r})=\frac{1}{\mathcal{J}}\boldsymbol{\ell}_{25}$	$\boldsymbol{\Lambda}_5(\boldsymbol{r})=\frac{\xi_4\boldsymbol{\ell}_{12}}{\mathcal{J}}$
$\boldsymbol{\Omega}_{12}(\boldsymbol{r})=\xi_3\nabla\xi_4$	$\nabla\times\boldsymbol{\Omega}_{12}(\boldsymbol{r})=\frac{1}{\mathcal{J}}\boldsymbol{\ell}_{34}$	
$\boldsymbol{\Omega}_{23}(\boldsymbol{r})=\xi_1\nabla\xi_4$	$\nabla\times\boldsymbol{\Omega}_{23}(\boldsymbol{r})=\frac{1}{\mathcal{J}}\boldsymbol{\ell}_{14}$	

The coordinates appearing in each dependency relation form a *group* of dependent coordinates. In listing the coordinates or indexes of interpolation points, it is convenient to highlight dependencies by writing groups of dependent coordinates together, with each group separated by a semicolon. All the independent quantities in a group are listed first so that the last variable in the group is the dependent one. Therefore, we list the coordinates as $\{\xi_1,\xi_2,\xi_3;\xi_4,\xi_5\}$ to put in evidence that ξ_1,ξ_2, and ξ_4 are the independent coordinates while ξ_3 and ξ_5 are dependent; we similarly list the indexes corresponding to sampled values of the coordinates as $\{i,j,k;\ell,m\}$ to put in evidence that k and m are dependent indexes.

The element edges are formed by intersection of pairs of zero-coordinates surfaces and the edge vectors are directed along the cross product of the associated coordinate gradients. The edges are given a two-index label deriving from the two coordinate indexes appearing in this cross product. The so-called *unitary basis vectors* $\boldsymbol{\ell}^1,\boldsymbol{\ell}^2,\boldsymbol{\ell}^4$ are derivatives of the element position vector with respect to the independent coordinates [1] and determine the following edge-vectors:

$$\begin{aligned}\boldsymbol{\ell}_{12}&=-\boldsymbol{\ell}_{13}=\boldsymbol{\ell}_{23}=\boldsymbol{\ell}^4\\ -\boldsymbol{\ell}_{14}&=\boldsymbol{\ell}_{15}=\boldsymbol{\ell}^2\\ \boldsymbol{\ell}_{24}&=-\boldsymbol{\ell}_{25}=\boldsymbol{\ell}^1\\ \boldsymbol{\ell}_{34}&=-\boldsymbol{\ell}_{35}=\boldsymbol{\ell}^2-\boldsymbol{\ell}^1.\end{aligned}\tag{2}$$

In the special case, where $\boldsymbol{\ell}^1$, $\boldsymbol{\ell}^2$, and $\boldsymbol{\ell}^4$ are constant vectors, the prism is a right prism.

The independent gradient vectors (or *reciprocal basis vectors*) $\nabla\xi_1$, $\nabla\xi_2$, $\nabla\xi_4$ are derived from (41) of [1]; the remaining coordinate gradients are determined by applying the gradient operator to (1) as $\nabla\xi_3=-\nabla\xi_1-\nabla\xi_2$, $\nabla\xi_5=-\nabla\xi_4$. For curvilinear elements, all these geometrical quantities, including the Jacobian $\mathcal{J}=\boldsymbol{\ell}^1\cdot\boldsymbol{\ell}^2\times\boldsymbol{\ell}^4$, vary with position.

By use of the Silvester polynomials $R_\alpha(q,\xi_\alpha)$ (see [1]), a Lagrange parameterization of order q for a curvilinear prism element can be expressed as

$$\begin{aligned}\boldsymbol{r}=\sum_{i,j,k,\ell,m=0}^{q}&\boldsymbol{r}_{ijk;\ell m}R_i(q,\xi_1)R_j(q,\xi_2)R_k(q,\xi_3)R_\ell(q,\xi_4)\\&\cdot R_m(q,\xi_5),\qquad i+j+k=\ell+m=q\end{aligned}\tag{3}$$

where the index quintuplet is used to label the position vector $\boldsymbol{r}_{ikj;\ell m}$ interpolating the point with normalized coordinates $\boldsymbol{\xi}_{(ijk;\ell m)}=(\xi_1,\xi_2,\xi_3;\xi_4,\xi_5)=(i/q,j/q,k/q;\ell/q,m/q)$.

III. CURL-CONFORMING INTERPOLATORY BASES ON PRISM ELEMENTS

A. Zeroth-Order Bases

Table I reports the zeroth-order curl-conforming bases $\boldsymbol{\Omega}_{ij}(\boldsymbol{r})$ on prism elements. Basis function $\boldsymbol{\Omega}_{ij}(\boldsymbol{r})$ interpolates the vector component tangent to the midpoint of the edge formed by the intersection of faces i and j. While the bases of Table I are unnormalized, their normalized forms are easily deduced from the normalized pth-order forms presented below upon setting $p=0$.

B. Completeness of Zeroth-Order Bases

Despite the appearance of linear and quadratic terms, the curl-conforming set of Table I is clearly complete only to zeroth-order since, for example, the set is unable to represent linear vectors of the form $\xi_i\nabla\xi_i$ $(i=1,2,4)$. Completeness to zeroth order follows from the following linear combinations which produce three independent constant vectors:

$$\begin{aligned}\boldsymbol{\Omega}_{24}(\boldsymbol{r})-\boldsymbol{\Omega}_{34}(\boldsymbol{r})-\boldsymbol{\Omega}_{25}(\boldsymbol{r})+\boldsymbol{\Omega}_{35}(\boldsymbol{r})&=\nabla\xi_1\\ \boldsymbol{\Omega}_{34}(\boldsymbol{r})-\boldsymbol{\Omega}_{14}(\boldsymbol{r})-\boldsymbol{\Omega}_{35}(\boldsymbol{r})+\boldsymbol{\Omega}_{15}(\boldsymbol{r})&=\nabla\xi_2\\ \boldsymbol{\Omega}_{12}(\boldsymbol{r})+\boldsymbol{\Omega}_{23}(\boldsymbol{r})-\boldsymbol{\Omega}_{13}(\boldsymbol{r})&=\nabla\xi_4.\end{aligned}\tag{4}$$

Note that $\nabla\xi_3=-\nabla\xi_1-\nabla\xi_2=\boldsymbol{\Omega}_{14}(\boldsymbol{r})-\boldsymbol{\Omega}_{24}(\boldsymbol{r})-\boldsymbol{\Omega}_{15}(\boldsymbol{r})+\boldsymbol{\Omega}_{25}(\boldsymbol{r})$.

Completeness of the curl of the bases to zeroth order follows from

$$\nabla \times \boldsymbol{\Omega}_{13}(\boldsymbol{r}) = \frac{\boldsymbol{\ell}_{25}}{\mathcal{J}}\left(= -\frac{\boldsymbol{\ell}^1}{\mathcal{J}}\right)$$
$$\nabla \times \boldsymbol{\Omega}_{23}(\boldsymbol{r}) = \frac{\boldsymbol{\ell}_{14}}{\mathcal{J}}\left(= -\frac{\boldsymbol{\ell}^2}{\mathcal{J}}\right)$$
$$\nabla \times [\boldsymbol{\Omega}_{34}(\boldsymbol{r}) - \boldsymbol{\Omega}_{35}(\boldsymbol{r})] = \frac{2\boldsymbol{\ell}_{12}}{\mathcal{J}}\left(= \frac{\boldsymbol{\ell}^4}{\mathcal{J}}\right). \tag{5}$$

On curvilinear elements, completeness is with respect to these vectors as weighting factors.

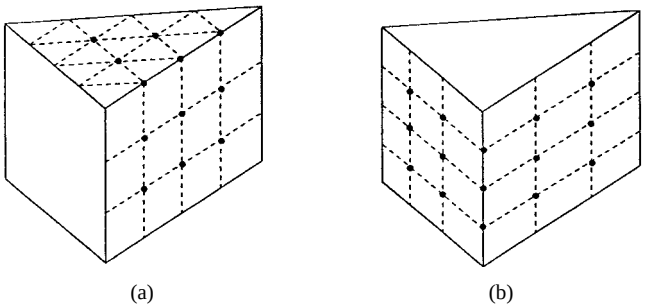

(a) (b)

Fig. 2. Interpolation points for curl-conforming bases of order $p = 2$ on prism elements (interior interpolation points omitted for clarity). (a) Nodes in basis subset $\boldsymbol{\Omega}^{15}_{ijk;\ell m}$. (b) Nodes in basis subset $\boldsymbol{\Omega}^{13}_{ijk;\ell m}$.

C. Order p Bases

Curl-conforming interpolating vector bases complete to order p on a prism element may be written as

$$\boldsymbol{\Omega}^{\gamma\beta}_{ijk;\ell m}(\boldsymbol{r}) = N^{\gamma\beta}_{ijk;\ell m}\frac{(p+1)\xi_\gamma\xi_\beta\hat{\alpha}^{\gamma\beta}_{ijk;\ell m}(\boldsymbol{\xi})}{\boldsymbol{i_\gamma i_\beta}}\boldsymbol{\Omega}_{\gamma\beta}(\boldsymbol{r}) \tag{6}$$

where i_γ is taken to be i, j, k, ℓ, or m for $\gamma = 1, 2, 3, 4$, or 5, respectively, and similarly for i_β. In (6), the ranges of γ and β are such as to include all the zeroth-order curl-conforming bases of Table I. The ranges on the remaining indexes i, j, k, ℓ, m are $\{1, 2, \cdots, p+1\}$, except for i_γ and i_β, whose ranges are $\{0, 1, \cdots, p\}$. The polynomial $\hat{\alpha}^{\gamma\beta}_{ijk;\ell m}(\boldsymbol{\xi})$ is defined in terms of shifted Silvester–Lagrange polynomials [1] as in (7), shown at the bottom of the page, with $\boldsymbol{\xi} = (\xi_1, \xi_2, \xi_3; \xi_4, \xi_5)$ and with

$$i + j + k = \begin{cases} (p+1), & \gamma\beta \in \{12, 13, 23\} \\ (p+2), & \text{otherwise} \end{cases}$$
$$\ell + m = \begin{cases} (p+2), & \gamma\beta \in \{12, 13, 23\} \\ (p+1), & \text{otherwise.} \end{cases} \tag{8}$$

The arrangement of interpolation points is similar to that of scalar Lagrange bases of the same order on a prism except that the pattern contracts away from the three faces where tangential components of the zeroth-order bases vanish. Notice that the zero in the interpolation polynomial along faces γ and β for interior nodes is explicitly exhibited in (6). For face or edge nodes, however, the denominator factors i_γ and/or i_β are also zero and [1, eq. (5)] together with (7) above must be used to evaluate the ratio. Conversely, for i_γ, i_β nonzero, the interpolation function $\hat{\alpha}^{\gamma\beta}_{ijk;\ell m}$ may be viewed as an ordinary Silvester–Lagrange polynomial of total order $2(p-1)$, with interpolation nodes shifted to the interior (as indicated by the caret).

Interpolation points for bases of the form $\boldsymbol{\Omega}^{15}_{ijk;\ell m}(\boldsymbol{r})$, $\boldsymbol{\Omega}^{13}_{ijk;\ell m}(\boldsymbol{r})$ are shown in Fig. 2(a) and (b), respectively. The arrangement of interpolation points for the remaining bases may be determined from the figures by rotating the pattern to put the edge interpolation points along a new edge. Note that no vertices of the prism element are interpolated and only a single basis function interpolates a component tangential to a given edge. The tangential components at each interpolation point on a face are interpolated by the bases containing as factors zeroth-order basis functions which are associated with the edges bounding that face. But on a face, only two of these tangential components can be independent. Hence two basis functions on rectangular faces and one basis function on triangular faces at each interpolation point must be eliminated. For interpolation points on rectangular faces, only pairs of basis functions with zeroth-order basis factors associated with edges bounding the face and having a common vertex should be eliminated. Similarly, on the interior, only three bases that interpolate each interior point should be retained to provide interpolation of the three independent components. One of these should have a zeroth-order basis factor associated with an edge formed by intersecting rectangular faces; the remaining two should have zeroth-order basis factors associated with any two edges of, say, one of the triangular faces. The dependency relations for face and interior nodes are given below.

The normalization constants in (6) are chosen to ensure that the component of $\boldsymbol{\Omega}^{\gamma\beta}_{ijk;\ell m}(\boldsymbol{r})$ along $\boldsymbol{\ell}_{\gamma\beta}$ at the interpolation point is unity. They are given by

$$N^{\gamma\beta}_{ijk;\ell m} = \begin{cases} \dfrac{(p+1)}{p+1-i_\gamma-i_\beta}\ell^{(ijk;\ell m)}_{\gamma\beta} \\ \quad \gamma\beta \in \{12, 13, 23\} \\ \dfrac{(p+1)(p+2)}{(p+2-i_\gamma)(p+1-i_\beta)}\ell^{(ijk;\ell m)}_{\gamma\beta} \\ \quad \text{otherwise} \end{cases} \tag{9}$$

where $\ell^{(ijk;\ell m)}_{\gamma\beta}$ is the value of $\ell_{\gamma\beta} = |\boldsymbol{\ell}_{\gamma\beta}|$ at the interpolation

$$\hat{\alpha}^{\gamma\beta}_{ijk;\ell m}(\boldsymbol{\xi}) = \begin{cases} (p+1)\hat{R}_i(p+1,\xi_1)\hat{R}_j(p+1,\xi_2)\hat{R}_k(p+1,\xi_3)\hat{R}_\ell(p+2,\xi_4)\hat{R}_m(p+2,\xi_5) \\ \quad \gamma\beta \in \{12, 13, 23\} \\ (p+2)\hat{R}_i(p+2,\xi_1)\hat{R}_j(p+2,\xi_2)\hat{R}_k(p+2,\xi_3)\hat{R}_\ell(p+1,\xi_4)\hat{R}_m(p+1,\xi_5) \\ \quad \text{otherwise;} \end{cases} \tag{7}$$

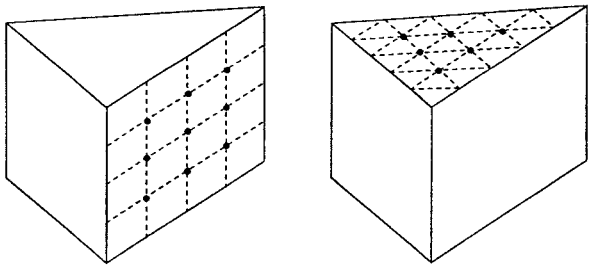

(a) (b)

Fig. 3. Interpolation points for divergence-conforming bases of order $p = 2$ on prism elements (interior interpolation points omitted for clarity). (a) Nodes in basis subset $\boldsymbol{\Lambda}^1_{ijk;\ell m}$. (b) Nodes in basis subset $\boldsymbol{\Lambda}^5_{ijk;\ell m}$.

point

$$\boldsymbol{\xi}^{\gamma\beta}_{(ijk;\ell m)} = \begin{cases} \left(\dfrac{i}{p+1}, \dfrac{j}{p+1}, \dfrac{k}{p+1}; \dfrac{\ell}{p+2}, \dfrac{m}{p+2}\right) \\ \qquad \gamma\beta \in \{12, 13, 23\} \\ \left(\dfrac{i}{p+2}, \dfrac{j}{p+2}, \dfrac{k}{p+2}; \dfrac{\ell}{p+1}, \dfrac{m}{p+1}\right) \\ \qquad \text{otherwise.} \end{cases} \tag{10}$$

As a matter of practical implementation, we note that the three linear combinations

$$\frac{\boldsymbol{\Omega}^{\beta+1,4}_{ijk;\ell m}(\boldsymbol{r})}{N^{\beta+1,4}_{ijk;\ell m}} - \frac{\boldsymbol{\Omega}^{\beta+1,5}_{ijk;\ell m}(\boldsymbol{r})}{N^{\beta+1,5}_{ijk;\ell m}} - \frac{\boldsymbol{\Omega}^{\beta-1,4}_{ijk;\ell m}(\boldsymbol{r})}{N^{\beta-1,4}_{ijk;\ell m}} + \frac{\boldsymbol{\Omega}^{\beta-1,5}_{ijk;\ell m}(\boldsymbol{r})}{N^{\beta-1,5}_{ijk;\ell m}} \tag{11}$$

for $\beta = 1, 2, 3$ and with index arithmetic performed modulo three reduce to $\nabla\xi_\beta$ at interior interpolation nodes; whereas the linear combination

$$\frac{\boldsymbol{\Omega}^{12}_{ijk;\ell m}(\boldsymbol{r})}{N^{12}_{ijk;\ell m}} + \frac{\boldsymbol{\Omega}^{23}_{ijk;\ell m}(\boldsymbol{r})}{N^{23}_{ijk;\ell m}} - \frac{\boldsymbol{\Omega}^{13}_{ijk;\ell m}(\boldsymbol{r})}{N^{13}_{ijk;\ell m}} \tag{12}$$

reduces to $\nabla\xi_4 = -\nabla\xi_5$ at interior nodes. Therefore, (12) together with any two of the three linear combinations (11), suitably renormalized, provide convenient alternative bases for interpolating interior points. On the quadrilateral face β $(= 1, 2, 3)$, the tangential components of $\nabla\xi_\beta$ and, hence, those of the corresponding linear combinations (11) vanish at the interpolation point; one of the two remaining combinations in (11) together with (12), however, can serve as convenient bases for interpolating nodes on face β $(= 1, 2, 3)$. Similarly, on the triangular face four or five, the tangential components of (12) vanish at the interpolation point and any two of the three combinations (11) can serve as bases for interpolating nodes on the triangular face. With (11), (12) interpolating interior and face nodes, and with (6) interpolating edge nodes, the degrees of freedom simply become the covariant vector components at each interpolation point. Since the bases are normalized and interpolate tangential components, it becomes trivial to enforce tangential continuity of fields across element boundaries.

D. Completeness to Order p in the Curl

Completeness in the curl follows as a consequence of the fact that the zeroth-order curl conforming functions contain linear terms able to model the following linear vectors:

$$\begin{aligned} \boldsymbol{\Upsilon}_1(\boldsymbol{r}) &= \xi_1\nabla\xi_4 - \xi_4\nabla\xi_1 = \boldsymbol{\Omega}_{23}(\boldsymbol{r}) + \boldsymbol{\Omega}_{25}(\boldsymbol{r}) - \boldsymbol{\Omega}_{35}(\boldsymbol{r}) \\ \boldsymbol{\Upsilon}_2(\boldsymbol{r}) &= \xi_2\nabla\xi_1 - \xi_1\nabla\xi_2 = \boldsymbol{\Omega}_{35}(\boldsymbol{r}) - \boldsymbol{\Omega}_{34}(\boldsymbol{r}) \\ \boldsymbol{\Upsilon}_4(\boldsymbol{r}) &= \xi_4\nabla\xi_2 - \xi_2\nabla\xi_4 = \boldsymbol{\Omega}_{13}(\boldsymbol{r}) + \boldsymbol{\Omega}_{15}(\boldsymbol{r}) - \boldsymbol{\Omega}_{35}(\boldsymbol{r}). \end{aligned} \tag{13}$$

In the Appendix, these vectors are used together with multiplying polynomials of inhomogeneous form to prove completeness to order p in the curl.

E. Dependency Relations at Face and Interior Nodes

As discussed following (8), only two of the three or four pth order bases for triangular or rectangular faces, respectively, which are nonvanishing at an interpolation point on a face, are independent. Similarly, only three bases that interpolate an interior point of the prism are independent. The dependencies arise from linear combinations of the bases that contain one of the following eight identities as factors:

$$\begin{aligned} \xi_1\boldsymbol{\Omega}_{1j}(\boldsymbol{r}) + \xi_2\boldsymbol{\Omega}_{2j}(\boldsymbol{r}) + \xi_3\boldsymbol{\Omega}_{3j}(\boldsymbol{r}) &= \boldsymbol{0}, \quad \text{for } j = 4, 5 \\ \xi_4\boldsymbol{\Omega}_{i4}(\boldsymbol{r}) + \xi_5\boldsymbol{\Omega}_{i5}(\boldsymbol{r}) &= \boldsymbol{0}, \quad \text{for } i = 1, 2, 3 \\ \xi_1\boldsymbol{\Omega}_{12}(\boldsymbol{r}) - \xi_3\boldsymbol{\Omega}_{23}(\boldsymbol{r}) &= \boldsymbol{0} \\ \xi_1\boldsymbol{\Omega}_{13}(\boldsymbol{r}) + \xi_2\boldsymbol{\Omega}_{23}(\boldsymbol{r}) &= \boldsymbol{0} \\ \xi_2\boldsymbol{\Omega}_{12}(\boldsymbol{r}) + \xi_3\boldsymbol{\Omega}_{13}(\boldsymbol{r}) &= \boldsymbol{0}. \end{aligned} \tag{14}$$

Indeed, at face and interior nodes the previous identities immediately yield

$$\left.\begin{aligned} &\frac{i\boldsymbol{\Omega}^{14}_{ijk;\ell m}(\boldsymbol{r})}{N^{14}_{ijk;\ell m}} + \frac{j\boldsymbol{\Omega}^{24}_{ijk;\ell m}(\boldsymbol{r})}{N^{24}_{ijk;\ell m}} + \frac{k\boldsymbol{\Omega}^{34}_{ijk;\ell m}(\boldsymbol{r})}{N^{34}_{ijk;\ell m}} = \boldsymbol{0} \\ &\frac{i\boldsymbol{\Omega}^{15}_{ijk;\ell m}(\boldsymbol{r})}{N^{15}_{ijk;\ell m}} + \frac{j\boldsymbol{\Omega}^{25}_{ijk;\ell m}(\boldsymbol{r})}{N^{25}_{ijk;\ell m}} + \frac{k\boldsymbol{\Omega}^{35}_{ijk;\ell m}(\boldsymbol{r})}{N^{35}_{ijk;\ell m}} = \boldsymbol{0} \end{aligned}\right\}, \quad \text{for } i, j, k \neq 0$$

$$\left.\begin{aligned} &\frac{\ell\boldsymbol{\Omega}^{14}_{ijk;\ell m}(\boldsymbol{r})}{N^{14}_{ijk;\ell m}} + \frac{m\boldsymbol{\Omega}^{15}_{ijk;\ell m}(\boldsymbol{r})}{N^{15}_{ijk;\ell m}} = \boldsymbol{0} \\ &\frac{\ell\boldsymbol{\Omega}^{24}_{ijk;\ell m}(\boldsymbol{r})}{N^{24}_{ijk;\ell m}} + \frac{m\boldsymbol{\Omega}^{25}_{ijk;\ell m}(\boldsymbol{r})}{N^{25}_{ijk;\ell m}} = \boldsymbol{0} \\ &\frac{\ell\boldsymbol{\Omega}^{34}_{ijk;\ell m}(\boldsymbol{r})}{N^{34}_{ijk;\ell m}} + \frac{m\boldsymbol{\Omega}^{35}_{ijk;\ell m}(\boldsymbol{r})}{N^{35}_{ijk;\ell m}} = \boldsymbol{0} \end{aligned}\right\}, \quad \text{for } \ell, m \neq 0$$

$$\begin{aligned} &\frac{i\boldsymbol{\Omega}^{12}_{ijk;\ell m}(\boldsymbol{r})}{N^{12}_{ijk;\ell m}} - \frac{k\boldsymbol{\Omega}^{23}_{ijk;\ell m}(\boldsymbol{r})}{N^{23}_{ijk;\ell m}} = \boldsymbol{0}, \quad \text{for } i, k \neq 0 \\ &\frac{i\boldsymbol{\Omega}^{13}_{ijk;\ell m}(\boldsymbol{r})}{N^{13}_{ijk;\ell m}} + \frac{j\boldsymbol{\Omega}^{23}_{ijk;\ell m}(\boldsymbol{r})}{N^{23}_{ijk;\ell m}} = \boldsymbol{0}, \quad \text{for } i, j \neq 0 \\ &\frac{j\boldsymbol{\Omega}^{12}_{ijk;\ell m}(\boldsymbol{r})}{N^{12}_{ijk;\ell m}} + \frac{k\boldsymbol{\Omega}^{13}_{ijk;\ell m}(\boldsymbol{r})}{N^{13}_{ijk;\ell m}} = \boldsymbol{0}, \quad \text{for } j, k \neq 0. \end{aligned} \tag{15}$$

F. Number of Degrees of Freedom

The number of degrees of freedom for curl-conforming bases of order p on a prism element may be determined as follows:

- one component $\times(p+1)$ DOF's $\times$ nine edges $= 9(p+1)$ edge degrees of freedom;
- two components $\times(p(p+1)/2)$ DOF's $\times$ two triangular faces $= 2p(p+1)$ face degrees of freedom;
- two components $\times p(p+1)$ DOF's $\times$ three rectangular faces $= 6p(p+1)$ face degrees of freedom;
- two components $\times(p^2(p+1)/2)$ interior DOF's $= p^2(p+1)$ prism interior degrees of freedom;
- one component $\times(p(p-1)(p+1)/2)$ interior DOF's $= (p(p-1)(p+1)/2)$ prism interior degrees of freedom

for a total of $3(p+1)(p+2)(p+3)/2$ degrees of freedom per prism element.

IV. Divergence-Conforming Bases on Prism Elements

A. Zeroth-Order Bases

Table I reports the unnormalized forms of the zeroth-order divergence-conforming bases $\boldsymbol{\Lambda}_i(\boldsymbol{r})$ on prism elements; their normalized forms are easily deduced from the normalized pth order forms presented below upon setting $p = 0$. Basis function $\boldsymbol{\Lambda}_i(\boldsymbol{r})$ interpolates the vector component normal to the centroid of face i. Although these zeroth-order bases contain linear terms, they are complete only to zeroth order. Completeness to zeroth order follows from the following linear combinations, which produce three independent constant vectors:

$$\begin{aligned}\boldsymbol{\Lambda}_2(\boldsymbol{r}) - \boldsymbol{\Lambda}_3(\boldsymbol{r}) &= \frac{\boldsymbol{\ell}_{14}}{\mathcal{J}}\left(= -\frac{\boldsymbol{\ell}^2}{\mathcal{J}}\right)\\ \boldsymbol{\Lambda}_3(\boldsymbol{r}) - \boldsymbol{\Lambda}_1(\boldsymbol{r}) &= \frac{\boldsymbol{\ell}_{24}}{\mathcal{J}}\left(= \frac{\boldsymbol{\ell}^1}{\mathcal{J}}\right)\\ \boldsymbol{\Lambda}_5(\boldsymbol{r}) - \boldsymbol{\Lambda}_4(\boldsymbol{r}) &= \frac{\boldsymbol{\ell}_{12}}{\mathcal{J}}\left(= \frac{\boldsymbol{\ell}^4}{\mathcal{J}}\right).\end{aligned} \tag{16}$$

On curvilinear prisms, completeness is with respect to these vectors as weighting factors.

Completeness of the divergence of the bases to zeroth order follows from

$$\nabla\cdot\boldsymbol{\Lambda}_i(\boldsymbol{r}) = \begin{cases}\dfrac{2}{\mathcal{J}}, & i = 1,2,3\\ \dfrac{1}{\mathcal{J}}, & i = 4,5.\end{cases} \tag{17}$$

Again, on curvilinear elements, completeness is with respect to $1/\mathcal{J}$ as a weighting factor.

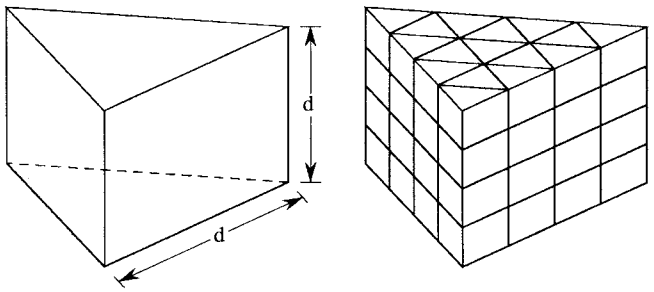

(a) (b)

Fig. 4. (a) Prism cavity. (b) Prism cavity discretized with 64 equilateral prisms.

B. Order p Bases

Divergence-conforming interpolatory vector bases complete to order p on a prism element are given by the following polynomial products with the zeroth-order bases of Table I:

$$\boldsymbol{\Lambda}^{\gamma}_{ijk;\ell m}(\boldsymbol{r}) = N^{\gamma}_{ijk;\ell m}\frac{\xi_\gamma\hat{\alpha}^{\gamma}_{ijk;\ell m}(\boldsymbol{\xi})}{i_{\boldsymbol{\gamma}}}\boldsymbol{\Lambda}_\gamma(\boldsymbol{r}),\quad \gamma = 1,2,\cdots,5 \tag{18}$$

where i_γ is taken to be i, j, k, ℓ, or m for $\gamma = 1, 2, 3, 4$, or 5, respectively. The ranges on the indexes i, j, k, ℓ, m are $\{1, 2, \cdots, p+1\}$, except for i_γ, whose range is $\{0, 1, \cdots, p\}$. The Silvester–Lagrange interpolating polynomial is (19), as shown at the bottom of the page, with

$$\begin{aligned} i+j+k &= \begin{cases}(p+2), & \gamma\in\{1,2,3\}\\ (p+3), & \gamma\in\{4,5\}\end{cases}\\ \ell+m &= \begin{cases}(p+2), & \gamma\in\{1,2,3\}\\ (p+1), & \gamma\in\{4,5\}.\end{cases}\end{aligned} \tag{20}$$

Interpolation points for bases of the form $\boldsymbol{\Lambda}^{1}_{ijk;\ell m}(\boldsymbol{r})$, $\boldsymbol{\Lambda}^{5}_{ijk;\ell m}(\boldsymbol{r})$ are shown in Fig. 3. The interpolation points are arranged similar to those of scalar Lagrange bases of the same order on a prism, except that the pattern contracts away from the four faces where normal components of the zeroth-order bases vanish. The arrangement of interpolation points for the remaining bases may be determined from the figure by rotating the pattern to put the face interpolation points along a new face. Note that no vertex or edge points of the prism element are interpolated and that only a single basis function interpolates a component normal to a given face. On the interior, only three of the five bases, which interpolate each interior point should be retained to provide interpolation of the three independent components. One of these should have a zeroth-order basis factor associated with a triangular face; the remaining two should have zeroth-order basis factors associated with any two of the rectangular faces. The dependency relations for interior nodes are given below.

In this case, the normalization constants are chosen to ensure that the component of $\boldsymbol{\Lambda}^{\gamma}_{ijk;\ell m}(\boldsymbol{r})$ along the height unit vector

$$\hat{\alpha}^{\gamma}_{ijk;\ell m}(\boldsymbol{\xi}) = \begin{cases}(p+2)\hat{R}_i(p+2,\xi_1)\hat{R}_j(p+2,\xi_2)\hat{R}_k(p+2,\xi_3)\hat{R}_\ell(p+2,\xi_4)\hat{R}_m(p+2,\xi_5), & \gamma\in\{1,2,3\}\\ (p+1)\hat{R}_i(p+3,\xi_1)\hat{R}_j(p+3,\xi_2)\hat{R}_k(p+3,\xi_3)\hat{R}_\ell(p+1,\xi_4)\hat{R}_m(p+1,\xi_5), & \gamma\in\{4,5\}\end{cases} \tag{19}$$

TABLE II
EIGENVALUES OF THE EQUILATERAL PRISM CAVITY OF FIG. 4(a)
COMPUTED WITH TENTH-ORDER COMPLETE FUNCTIONS

modal order number	mode; degeneracy	kd exact	kd numerical	% error
1	$TE_{0,1,(-1),1}$ 2	$\frac{5}{3}\pi$	5.2359877666	2.0×10^{-7}
2			5.2359878015	8.7×10^{-7}
3	$TM_{1,1,(-2),0}$	$\frac{4}{\sqrt{3}}\pi$	7.2551974558	-1.6×10^{-8}
4	$TE_{0,1,(-1),2}$ 2	$\frac{2\sqrt{13}}{3}\pi$	7.5514489320	-1.0×10^{-8}
5			7.5514489354	3.6×10^{-8}
6	$TM_{1,1,(-2),1}$	$\sqrt{\frac{19}{3}}\pi$	7.9061681227	-1.2×10^{-7}
7	$TE_{1,1,(-2),1}$		7.9061681346	2.6×10^{-8}
8	$TE_{0,2,(-2),1}$ 2	$\frac{\sqrt{73}}{3}\pi$	8.9472598127	1.5×10^{-7}
9			8.9472698179	2.1×10^{-7}
10	$TM_{1,1,(-2),2}$	$\frac{2\sqrt{21}}{3}\pi$	9.5977240908	-1.2×10^{-8}
11	$TE_{1,1,(-2),2}$		9.5977241043	1.3×10^{-7}
12	$TE_{0,1,(-1),3}$ 2	$\frac{\sqrt{97}}{3}\pi$	10.313700246	4.6×10^{-6}
13			10.313700250	4.6×10^{-6}
14	$TE_{0,2,(-2),2}$ 2	$\frac{10}{3}\pi$	10.471975510	-2.3×10^{-8}
15			10.471975518	5.5×10^{-8}
16	$TM_{1,2,(-3),0}$ 2	$\frac{4\sqrt{7}}{3}\pi$	11.08249777	5.4×10^{-6}
17			11.08249781	5.7×10^{-6}
18			11.51917367	5.3×10^{-6}
19	$TM_{1,2,(-3),1}$ 2	$\frac{11}{3}\pi$	11.51917367	5.3×10^{-6}
20	$TE_{1,2,(-3),1}$ 2		11.51917370	5.5×10^{-6}
21			11.51917373	5.7×10^{-6}
⋮	⋮	⋮	⋮	⋮
55	$TM_{2,2,(-4),2}$	$2\sqrt{\frac{19}{3}}\pi$	15.812333	-2.1×10^{-5}
56	$TE_{2,2,(-4),2}$		15.812351	9.3×10^{-5}
57	$TE_{0,1,(-1),5}$ 2	$\frac{\sqrt{241}}{3}\pi$	16.266	5.7×10^{-2}
58			16.266	5.7×10^{-2}
59			16.3579	9.3×10^{-4}
60	$TM_{1,3,(-4),2}$ 2	$2\sqrt{\frac{61}{3}}\pi$	16.3579	9.3×10^{-4}
61	$TE_{1,3,(-4),2}$ 2		16.3581	1.9×10^{-3}
62			16.3581	1.9×10^{-3}

$\hat{\boldsymbol{h}}_\gamma$ at the interpolation point is unity. They are given by

$$N^{\gamma}_{ijk;\ell m} = \begin{cases} \dfrac{p+2}{p+2-i_\gamma} h_\gamma^{ijk;\ell m}, & \gamma \in \{1,2,3\} \\ \dfrac{p+1}{p+1-i_\gamma} h_\gamma^{ijk;\ell m}, & \gamma \in \{4,5\} \end{cases} \tag{21}$$

where $h_\gamma^{ijk;\ell m}$ is the value of $\mathcal{J}/|\boldsymbol{h}_\gamma|$ at the interpolation point

$$\boldsymbol{\xi}^{\gamma}_{(ijk;\ell m)} = \begin{cases} \left(\dfrac{i}{p+2}, \dfrac{j}{p+2}, \dfrac{k}{p+2}; \dfrac{\ell}{p+2}, \dfrac{m}{p+2}\right) \\ \gamma \in \{1,2,3\} \\ \left(\dfrac{i}{p+3}, \dfrac{j}{p+3}, \dfrac{k}{p+3}; \dfrac{\ell}{p+1}, \dfrac{m}{p+1}\right) \\ \gamma \in \{4,5.\} \end{cases} \tag{22}$$

To ensure continuity of the normal component of a face-node basis across elements, it is only necessary to adjust its sign to correspond to an arbitrarily selected reference direction across adjacent elements.

C. Completeness to Order p in the Divergence

Completeness to order p in the divergence is most easily shown using an inhomogeneous multiplying polynomial of order p [1]. In this case, completeness follows from the fact that terms of like order are generated. The divergence of the product of the zeroth-order bases and the pth order polynomial is found to be

$$\begin{aligned} \nabla \cdot \xi_2^\alpha \xi_3^\beta \xi_j^\gamma \boldsymbol{\Lambda}_1(\boldsymbol{r}) &= (\alpha+\beta+2)\frac{\xi_2^\alpha \xi_3^\beta \xi_j^\gamma}{\mathcal{J}}, \qquad j = 4,5 \\ \nabla \cdot \xi_3^\alpha \xi_1^\beta \xi_j^\gamma \boldsymbol{\Lambda}_2(\boldsymbol{r}) &= (\alpha+\beta+2)\frac{\xi_3^\alpha \xi_1^\beta \xi_j^\gamma}{\mathcal{J}}, \qquad j = 4,5 \\ \nabla \cdot \xi_1^\alpha \xi_2^\beta \xi_j^\gamma \boldsymbol{\Lambda}_3(\boldsymbol{r}) &= (\alpha+\beta+2)\frac{\xi_1^\alpha \xi_2^\beta \xi_j^\gamma}{\mathcal{J}}, \qquad j = 4,5 \\ \nabla \cdot \xi_1^\alpha \xi_2^\beta \xi_3^\gamma \xi_5^\delta \boldsymbol{\Lambda}_4(\boldsymbol{r}) &= (\delta+1)\frac{\xi_1^\alpha \xi_2^\beta \xi_3^\gamma \xi_5^\delta}{\mathcal{J}} \\ \nabla \cdot \xi_1^\alpha \xi_2^\beta \xi_3^\gamma \xi_4^\delta \boldsymbol{\Lambda}_5(\boldsymbol{r}) &= (\delta+1)\frac{\xi_1^\alpha \xi_2^\beta \xi_3^\gamma \xi_4^\delta}{\mathcal{J}}. \end{aligned} \tag{23}$$

For curvilinear prisms for which $\mathcal{J}$ is not a constant, polynomial completeness is with respect to $1/\mathcal{J}$ as a weighting factor.

D. Dependency Relations at Interior Nodes

As discussed following (20), only three of the pth order bases that are nonvanishing at an interior interpolation point

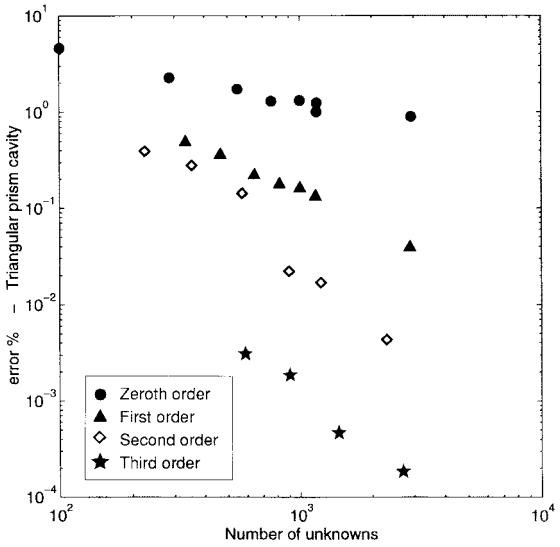

Fig. 5. Average error in computation of first nine resonant frequencies versus number of unknowns for a conducting prism cavity.

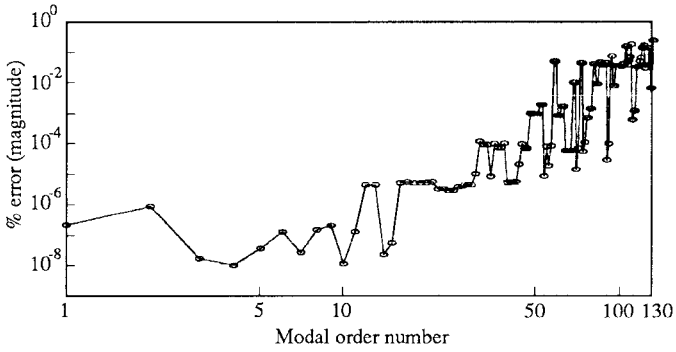

Fig. 6. Error in computation of resonant frequencies versus the modal order number for the conducting prism cavity of Fig. 4(a) studied with complete vector basis functions of order ten.

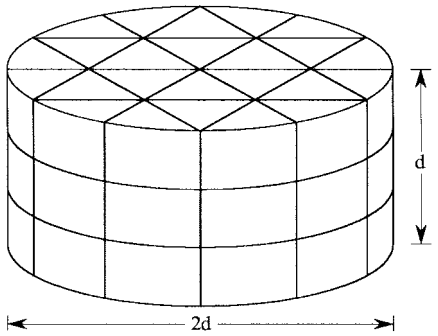

Fig. 7. Circular cylinder cavity discretized with 72 prism elements.

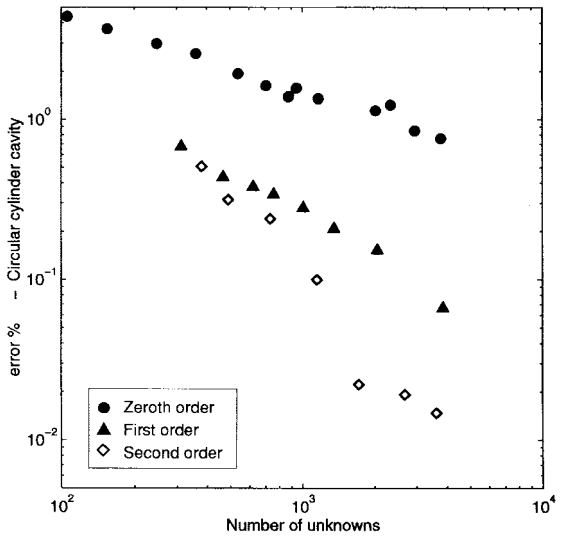

Fig. 8. Average error in computation of first eight resonant frequencies versus number of unknowns for a conducting circular cylinder cavity.

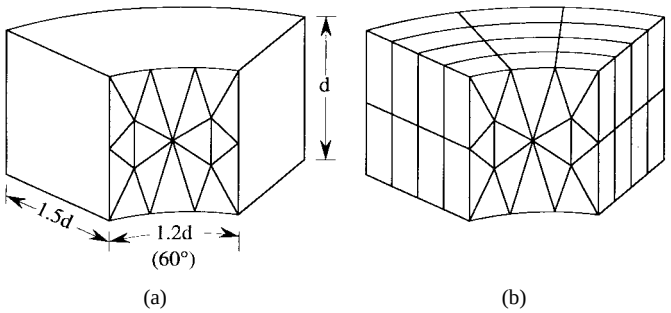

Fig. 9. Discretization of a pie-shell cavity. (a) A triangular mesh is defined on one face of the structure. (b) Seventy-two prism elements are then obtained by extrusion.

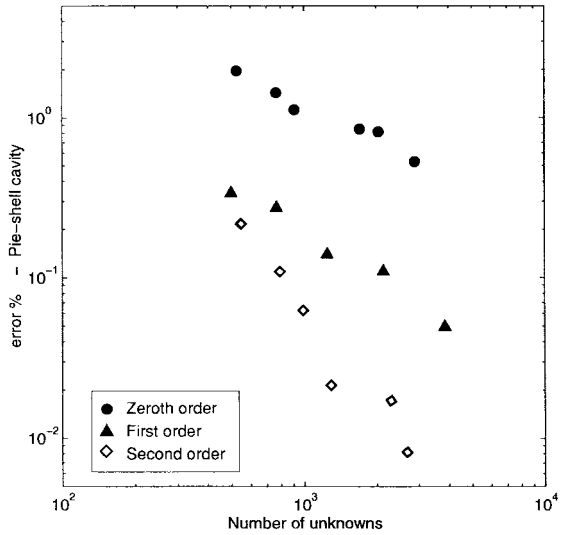

Fig. 10. Average error in computation of first eight resonant frequencies versus number of unknowns for a conducting pie-shell cavity.

are independent. The dependencies arise from linear combinations of the bases which contain the following identities as factors:

$$\xi_1 \boldsymbol{\Lambda}_1(\boldsymbol{r}) + \xi_2 \boldsymbol{\Lambda}_2(\boldsymbol{r}) + \xi_3 \boldsymbol{\Lambda}_3(\boldsymbol{r}) = \mathbf{0}$$
$$\xi_4 \boldsymbol{\Lambda}_4(\boldsymbol{r}) + \xi_5 \boldsymbol{\Lambda}_5(\boldsymbol{r}) = \mathbf{0}. \tag{24}$$

Indeed, at interior nodes the previous identities immediately yield

$$\frac{i\boldsymbol{\Lambda}^1_{ijk;\ell m}(\boldsymbol{r})}{N^1_{ijk;\ell m}} + \frac{j\boldsymbol{\Lambda}^2_{ijk;\ell m}(\boldsymbol{r})}{N^2_{ijk;\ell m}} + \frac{k\boldsymbol{\Lambda}^3_{ijk;\ell m}(\boldsymbol{r})}{N^3_{ijk;\ell m}} = \mathbf{0}, \quad \text{for } i, j, k \neq 0$$
$$\frac{\ell\boldsymbol{\Lambda}^4_{ijk;\ell m}(\boldsymbol{r})}{N^4_{ijk;\ell m}} + \frac{m\boldsymbol{\Lambda}^5_{ijk;\ell m}(\boldsymbol{r})}{N^5_{ijk;\ell m}} = \mathbf{0}, \quad \text{for } \ell, m \neq 0. \tag{25}$$

E. Number of Degrees of Freedom

The number of degrees of freedom for divergence-conforming bases of order p on a prism element may be determined as follows:

- one component $\times((p+1)(p+2)/2)$ DOF's $\times$ two faces plus one component $\times(p+1)^2$ DOF's $\times$ three faces $= (p+1)(4p+5)$ face degrees of freedom;
- two components $\times(p(p+1)^2/2)$ plus one component $\times(p(p+1)(p+2)/2)$ interior DOF's $= (p(p+1)(3p+4)/2)$ prism interior degrees of freedom

for a total of $(p+1)(3p^2+12p+10)/2$ degrees of freedom.

V. Numerical Results

Here, we present some results to illustrate the benefits of using higher order vector bases on prism elements. The examples we consider are relative to resonant cavities, where the resonant frequencies were determined by finding the eigenvalues of the discretized vector Helmholtz equation involving the cavity electric field [5]. A Galerkin form of the finite-element method was used to discretize the Helmholtz equation and curl-conforming bases on triangular prisms were used to model each cavity; curvilinear prisms with quadratic distortion were used on the cavity boundary when necessary.

The first geometry we consider is the prism cavity shown in Fig. 4. The cavity has an equilateral triangular base and the height d of the cavity is equal to the length of the triangular side [Fig. 4(a)]. Fig. 4(b) shows a discretization of

this cavity with 64 equilateral prisms; the cavity problem of Fig. 4(b) yields 644 and 2310 unknowns when first and second order elements are used, respectively. This problem is an ideal test case to assess the performance of curl-conforming functions on prism elements of different order because there is no need to distort the elements in order to match the geometry and, hence, equilateral cells can be used. The analytical solution of this waveguide problem is apparently due to Schwinger (unpublished lecture notes on electromagnetic fields in waveguides) and is reported in detail in [6]. In [6], the modes of the triangular waveguide are labeled with three indexes ($\ell, m, n,$ with $\ell + m + n = 0$); we adopt Schwinger's notation, thereby labeling the cavity modes with four indexes (as in Table II), where the fourth index denotes the number of oscillations along the axis of the cavity. Fig. 5 is a plot of the error in the computed resonant frequencies of the prism cavity versus the number of unknowns. The error is averaged over the first nine eigenfrequencies, which include eight degenerate modes. From this figure one can appreciate the faster convergence of the results for increasing order p of the vector bases. Asymptotically, for a given p and decreasing mesh size s, the error appears to behave as $s^{2(p+1)}$. However, the quality of the results strictly depends on the *quality* of the mesh and this can also be appreciated in Fig. 5 since it was not always possible to use equilateral cells.

The same cavity problem was solved with vector bases of order ten defined on the single element of Fig. 4(a) so that the functions were actually entire-domain vector bases. The total number of degrees of freedom for this single element of order ten is 2574, yielding a fully populated system of equations with 1595 unknowns (number of interior degrees of freedom). In this connection, it is important to observe that the sparsity of the finite-element matrices decreases for increasing order of the bases while higher accuracy is required in the integration routines used to compute the matrix coefficients. As a matter of fact, in general applications, it is usually convenient, as a rule of thumb, to work with vector bases of no higher than third or fourth order. Nevertheless, we present the results of Table II to prove that our construction scheme can easily be applied to arbitrarily high orders. In this case, we obtained 450 zero eigenvalues and our numerical code was able to clearly distinguish the first 130 modes. No spurious nonzero eigenvalues were observed. As shown in Fig. 6, for the first thirty modes the percentage error is less than 10^{-5} and it remains always below the 10^{-4} level up to the 46th mode.

The second test case is a circular cavity of radius and height equal to d, discretized as in Fig. 7 by defining a triangular mesh on one of the cylinder bases and then by extruding these triangles into prism cells. The mesh of Fig. 7 consists of 72 prism cells, which yields systems of 762 and 2691 unknowns for $p = 1$ and 2, respectively. The percentage errors in the computed resonant frequencies versus the number of unknowns are reported in Fig. 8 for $p = 0, 1,$ and 2; the reported error is averaged over the first eight eigenfrequencies, which include six degenerate modes.

Finally, we studied the pie-shell cavity of Fig. 9(a). The 3-D mesh is obtained by first defining a triangular mesh on a parent rectangle having one side of length d and the other of length $1.2d$; this planar mesh is then *smeared* on one curved face of the pie shell [Fig. 9(a)] and, finally, by extrusion, the prism mesh of Fig. 9(b) is obtained. The mesh of Fig. 9(b), which, by the way, is not optimum consists of 72 triangular prisms; this yields systems of 776 and 2718 unknowns for $p = 1$ and 2, respectively. The numerical error for the first eight computed eigenfrequencies (eight nondegenerate modes) of this structure is reported in Fig. 10 for $p = 0, 1,$ and 2.

VI. Conclusions

This paper presents curl-conforming and divergence-conforming vector basis functions of the Nedelec variety for prism elements. The functions, which are derived for arbitrary polynomial order, can be consistently used to deal with curvilinear elements. Properties of the vector basis functions are discussed in detail. The reported numerical examples show that higher order functions provide more accurate results than those obtainable with low-order elements.

Appendix
Completeness in the Curl for Higher Order Curl-Conforming Bases

Using polynomials of inhomogeneous form [1], we first observe that any polynomial vector of order $(p + 1)$ can be expressed as the sum of a curl-free vector of order $(p+1)$ plus a vector, which can be represented in terms of curl-conforming functions of order p

$$\begin{aligned}
&(p+2)\xi_1^\alpha\xi_2^\beta\xi_4^\gamma\boldsymbol{\nabla}\xi_1 \\
&\quad = \boldsymbol{\nabla}(\xi_1^{\alpha+1}\xi_2^\beta\xi_4^\gamma) + \beta\xi_1^\alpha\xi_2^{\beta-1}\xi_4^\gamma\boldsymbol{\Upsilon}_2 - \gamma\xi_1^\alpha\xi_2^\beta\xi_4^{\gamma-1}\boldsymbol{\Upsilon}_1 \\
&(p+2)\xi_1^\alpha\xi_2^\beta\xi_4^\gamma\boldsymbol{\nabla}\xi_2 \\
&\quad = \boldsymbol{\nabla}(\xi_1^\alpha\xi_2^{\beta+1}\xi_4^\gamma) + \gamma\xi_1^\alpha\xi_2^\beta\xi_4^{\gamma-1}\boldsymbol{\Upsilon}_4 - \alpha\xi_1^{\alpha-1}\xi_2^\beta\xi_4^\gamma\boldsymbol{\Upsilon}_2 \\
&(p+2)\xi_1^\alpha\xi_2^\beta\xi_4^\gamma\boldsymbol{\nabla}\xi_4 \\
&\quad = \boldsymbol{\nabla}(\xi_1^\alpha\xi_2^\beta\xi_4^{\gamma+1}) + \alpha\xi_1^{\alpha-1}\xi_2^\beta\xi_4^\gamma\boldsymbol{\Upsilon}_1 - \beta\xi_1^\alpha\xi_2^{\beta-1}\xi_4^\gamma\boldsymbol{\Upsilon}_4 \\
&\qquad p = \alpha+\beta+\gamma-1 \geq 0, \\
&\qquad \alpha,\beta,\gamma \geq 0
\end{aligned} \tag{26}$$

where the vectors $\boldsymbol{\Upsilon}_1$, $\boldsymbol{\Upsilon}_2$, $\boldsymbol{\Upsilon}_4$ defined in (13), are linear combinations of curl-conforming bases.[1] Note that vectors $\boldsymbol{\nabla}(\xi_1^{\alpha+1}\xi_2^\beta\xi_4^\gamma)$, $\boldsymbol{\nabla}(\xi_1^\alpha\xi_2^{\beta+1}\xi_4^\gamma)$, and $\boldsymbol{\nabla}(\xi_1^\alpha\xi_2^\beta\xi_4^{\gamma+1})$ of order $(p+1)$ are the gradients of inhomogeneous polynomials of order $(p + 2)$ and, because they are gradients, are curl-free. Taking the curl of both sides of (26), one finds that the curl of any vector of order $(p + 1)$ (yielding a vector of order p) can always be expressed as a linear combination of the curl of curl-conforming bases of order p. Hence, the curl of curl-conforming bases of order p are complete to order p within the space of vectors derivable from the curl of vectors of order

[1] This proof also applies to tetrahedral and brick element functions; in these cases one has only to replace ξ_4 by ξ_3 and $\boldsymbol{\Upsilon}_4$ by $\boldsymbol{\Upsilon}_3 = \xi_3\boldsymbol{\nabla}\xi_2 - \xi_2\boldsymbol{\nabla}\xi_3$ in (26) since ξ_3 is the third independent variable used to define those cells [1]. Obviously, in those cases, one has to express the vector functions $\boldsymbol{\Upsilon}_1$, $\boldsymbol{\Upsilon}_2$, and $\boldsymbol{\Upsilon}_3$ in terms of the relevant zeroth-order bases.

$p+1$. These bases appear in inhomogeneous polynomial form in (26), but they are, of course, linear combinations of the interpolatory polynomial bases defined in (6).

REFERENCES

[1] R. D. Graglia, D. R. Wilton, and A. F. Peterson, "Higher order interpolatory vector bases for computational electromagnetics," *IEEE Trans. Antennas Propagat.—Special Issue Adv. Numer. Tech. Electromagn.*, vol. 45, pp. 329–342, Mar. 1997.

[2] J. C. Nedelec, "Mixed finite elements in R^3," *Numer. Math.*, vol. 35, pp. 315–341, 1980.

[3] D. R. Wilton, R. D. Graglia, and A. F. Peterson, "Higher order interpolatory vector bases for computational electromagnetics," Dept. Elect. Comput. Eng., Univ. Houston, TX, Final Rep. Sandia Nat. Lab., Contract AN9938, 1997.

[4] T. Özdemir and J. L. Volakis, "Triangular prisms for edge-based vector finite element analysis of conformal antennas," *IEEE Trans. Antennas Propagat.*, vol. 45, pp. 788–797, May 1997.

[5] I.-L. Gheorma and R. D. Graglia, "Higher order vectorial modeling using curvilinear prism elements," in *Proc. 5th Int. Conf. Electromagn. Aerosp. Applicat. (ICEAA)*, Torino, Italy, Sept. 1997, pp. 179–182.

[6] F. E. Borgnis and C. H. Papas, "Electromagnetic waveguides and resonators, Section C: Cylindrical waveguides," in *Encyclopedia of Physics: Electric Fields and Waves*, S. Flügge, Ed. Berlin, Germany: Springer-Verlag, 1958, vol. XVI, pp. 336–345 [subsection 16 (equilateral triangular waveguide) and 17 (other cylindrical waveguides of simple cross-section)].

Roberto D. Graglia (S'83–M'83–SM'90–F'98), for photograph and biography, see p. 314 of the March 1997 issue of this TRANSACTIONS.

Donald R. Wilton (S'63–M'65–SM'80–F'87), for photograph and biography, see p. 315 of the March 1997 issue of this TRANSACTIONS.

Andrew F. Peterson (S'82–M'83–SM'92), for photograph and biography, see p. 342 of the March 1997 issue of this TRANSACTIONS.

Ioan-Ludovic Gheorma was born in Dej, Romania, in 1966. He received the M.S.E.E. degree (with honors) from the Politehnica University of Bucharest, Romania, in 1997.

As a student, he worked in the field of vector FEM at the Numerical Methods Laboratory (LMN) of the Electrical Engineering Faculty of the Politechnic of Bucharest under a three-year research grant from the Japan Society of Applied Electromagnetics and Mechanics (JSAEM). In 1997 he was part of a Tempus-JEP Mobility Program at Politecnico di Torino, Italy. His areas of interest include numerical methods and computational electromagnetics.